

1 Atmospheric Oxidation Mechanism and Kinetics of Indole Initiated 2 by $\cdot\text{OH}$ and $\cdot\text{Cl}$: A Computational Study

3 Jingwen Xue^{1#}, Fangfang Ma^{1*}, Jonas Elm², Jingwen Chen¹, Hong-Bin Xie^{1*}

4 ¹Key Laboratory of Industrial Ecology and Environmental Engineering (Ministry of Education), School of Environmental
5 Science and Technology, Dalian University of Technology, Dalian 116024, China

6 ²Department of Chemistry and iClimate, Aarhus University, Langelandsgade 140, DK-8000 Aarhus C, Denmark

7 *Correspondence to:* Fang-Fang Ma (maff@dlut.edu.cn); Hong-Bin Xie (hbxie@dlut.edu.cn)

8 **Abstract.** The atmospheric chemistry of organic nitrogen compounds (ONCs) is of great importance for understanding the
9 formation of carcinogenic nitrosamines, and ONC oxidation products might influence atmospheric aerosol particle formation
10 and growth. Indole is a polyfunctional heterocyclic secondary amine with global emission quantity almost equivalent to that
11 of trimethylamine, the amine with the highest atmospheric emission. However, the atmospheric chemistry of indole remains
12 unclear. Herein, the reactions of indole with $\cdot\text{OH}/\cdot\text{Cl}$, and subsequent reactions of resulting indole-radicals with O_2 under 200
13 ppt NO and 50 ppt $\text{HO}_2\cdot$ conditions, were investigated by a combination of quantum chemical calculations and kinetics
14 modeling. The results indicate that $\cdot\text{OH}$ addition is the dominant pathway for the reaction of $\cdot\text{OH}$ with indole. However, both
15 $\cdot\text{Cl}$ addition and H-abstraction are feasible for the corresponding reaction with $\cdot\text{Cl}$. All favorably formed indole-radicals further
16 react with O_2 to produce peroxy radicals, which mainly react with NO and $\text{HO}_2\cdot$ to form organonitrates, alkoxy radicals and
17 hydroperoxide products. Therefore, the oxidation mechanism of indole is distinct from that of previously reported amines,
18 which primarily form highly oxidized multifunctional compounds, imines or carcinogenic nitrosamines. In addition, the peroxy
19 radicals from the $\cdot\text{OH}$ reaction can form N-(2-formylphenyl)formamide ($\text{C}_8\text{H}_7\text{NO}_2$), for the first time providing evidence for
20 the chemical identity of the $\text{C}_8\text{H}_7\text{NO}_2$ mass peak observed in the $\cdot\text{OH}$ + indole experiments. More importantly, this study is
21 the first to demonstrate that despite forming radicals by abstracting an H-atom at the N-site, carcinogenic nitrosamines were
22 not produced in the indole oxidation reaction.

23 1 Introduction

24 Volatile organic compounds (VOCs) play a central role in air quality and climate change as their transformations are
25 highly relevant for the formation of secondary organic aerosols (SOA), toxic air pollutants and ozone (O_3) (Ehn et al., 2014;
26 Karl et al., 2018; Lewis Alastair, 2018; Li et al., 2019; Khare and Gentner, 2018; Ji et al., 2018). Therefore, an accurate
27 description of the atmospheric transformation mechanism and kinetics of VOCs is essential to fully explore the global impacts
28 of VOCs. Despite massive effort to understand the atmospheric fate of VOCs, current mechanism-based atmospheric models
29 often underestimate SOA and O_3 formation quantity. Therefore, the emission inventories or reaction mechanism employed in

30 the models are either missing some vital primary VOCs or there remain unrevealed reaction mechanism of currently known
31 VOCs. Hence, it is crucial to identify unaccounted reaction pathways of known VOCs or transformation mechanism of
32 unconsidered VOCs with high concentrations.

33 Organic nitrogen compounds (ONCs) are a subgroup of VOCs that are widely observed in the atmosphere (Silva et al.,
34 2008). Until now, about 160 ONCs have been detected in the atmosphere, accounting for 10% of total gas phase nitrogen
35 (excluding N₂) (Ge et al., 2011; Silva et al., 2008). Due to the adverse effects of ONCs on air quality (formation of particles
36 via acid-base reactions or generation of toxic nitrosamines, nitramines, isocyanic acid and low volatile products via gas phase
37 oxidation), the chemistry of ONCs has gained significant attention in the recent years (Almeida et al., 2013; Chen et al., 2017;
38 Lin et al., 2019; Nielsen et al., 2012; Zhang et al., 2015; Xie et al., 2014; Xie et al., 2015; Xie et al., 2017; Ma et al., 2018a;
39 Ma et al., 2021a; Ma et al., 2019; Shen et al., 2019; Shen et al., 2020). Detailed transformation pathways of a series of ONCs
40 including low-molecular-weight alkyl amines (Nicovich et al., 2015; Xie et al., 2014; Xie et al., 2015; Ma et al., 2021a),
41 aromatic aniline (Xie et al., 2017; Shiels et al., 2021), heterocyclic amines (Sengupta et al., 2010; Ma et al., 2018a; Borduas et
42 al., 2016; Ren and Da Silva, 2019) and amides (Xie et al., 2017; Borduas et al., 2016; Borduas et al., 2015; Bunkan et al., 2016;
43 Bunkan et al., 2015) have been investigated. These studies have shown that the functional groups connected to the NH_x ($x = 0,$
44 $1, 2$) group highly affect the reactivity of ONCs and eventually lead to their different atmospheric impacts. Therefore, the
45 comprehensive understanding the reaction mechanism of ONCs with various functional groups linked to the NH_x group is of
46 great significance to assess the atmospheric impact of ONCs.

47 Indole is a polyfunctional heterocyclic secondary amine (Laskin et al., 2009). Atmospheric indole has various natural and
48 anthropogenic sources including vegetation, biomass burning, animal husbandry, coal mining, petroleum processing and
49 tobacco industry (Ma et al., 2021b; Cardoza et al., 2003; Yuan et al., 2017; Zito et al., 2015). The global emission of indole is
50 around 0.1 Tg yr⁻¹ (Misztal et al., 2015), which is almost equivalent to that of trimethylamine (~ 0.17 Tg yr⁻¹) (Schade and
51 Crutzen, 1995; Yu and Luo, 2014) which has the highest emission among the identified atmospheric amines. A field
52 measurement study found that the concentration of indole can reach 1-3 ppb in ambient air during a springtime flowering event
53 (Gentner et al., 2014). From a structural point of view, the -NH- group of indole is located at 9-center-10-electron delocalized
54 π bonds, possibly altering its reactivity compared to that of previously well-studied aliphatic amines and aniline. Therefore,
55 considering the large atmospheric emission of indole and its unique structure compared to previously studied amines, the
56 reaction mechanism of indole needs to be further evaluated to assess its atmospheric impacts. Furthermore, elucidating the
57 reaction mechanism of indole will add to the fundamental understanding of the transformation mechanism of ONCs.

58 Hydroxyl radicals ($\cdot\text{OH}$) are considered to be the most important atmospheric oxidants governing the fate of most organic
59 compounds (Macleod et al., 2007). Previous experimental studies have investigated the reaction kinetics and identified the
60 products of the $\cdot\text{OH} + \text{indole}$ reaction. Atkinson et al. found that the rate constant (k_{OH}) of the $\cdot\text{OH} + \text{indole}$ reaction is $1.54 \times$
61 $10^{-10} \text{ cm}^3 \text{ molecule}^{-1} \text{ s}^{-1}$ at 298 K, translating to a 20 min lifetime of indole (Atkinson et al., 1995). Montoya-Aguilera et al.
62 found that isatin and isatoic anhydride are the two dominate monomeric products for $\cdot\text{OH}$ initiated reaction of indole. More
63 importantly, they found that the majority of indole oxidation products can contribute to SOA formation with an effective SOA

64 yield of 1.3 ± 0.3 under the indole concentration (200 ppb) employed in their chamber study (Montoya-Aguilera et al., 2017).
65 Although the chemical formulas of some of the indole oxidation products have been detected, detailed mechanistic information
66 such as the products branching ratio of the $\cdot\text{OH}$ initiated reaction of indole remains unknown. Additionally, the lack of
67 commercially available standards of some products presents a significant obstacle to identify the exact chemical identity of the
68 products. Therefore, to fully understand the role of indole in SOA formation, it is essential to investigate the detailed
69 atmospheric transformation of indole initiated by $\cdot\text{OH}$.

70 Besides reactions with $\cdot\text{OH}$, reactions with chlorine radicals ($\cdot\text{Cl}$) have been proposed to be an important removal pathway
71 for ONCs due to the identification of new $\cdot\text{Cl}$ continental sources and the high reactivity of $\cdot\text{Cl}$ (Wang et al., 2022; Li et al.,
72 2021; Jahn et al., 2021; Xia et al., 2020; Young et al., 2014; Faxon and Allen, 2013; Riedel et al., 2012; Atkinson et al., 1989;
73 Ji et al., 2013; Thornton et al., 2010; Le Breton et al., 2018). $\cdot\text{Cl}$ initiated atmospheric oxidation of ONCs can lead to the
74 formation of N-centered radicals, once a strong 2-center-3-electron (2c-3e) bond complex has been formed between $\cdot\text{Cl}$ and
75 NH_x ($x = 1, 2$) (Mckee et al., 1996; Xie et al., 2015; Xie et al., 2017; Ma et al., 2018a). The formed N-centered radicals can
76 further react with NO to form carcinogenic nitrosamines, increasing the atmospheric impact of ONC emissions (Xie et al.,
77 2014; Xie et al., 2015; Xie et al., 2017; Ma et al., 2018a; Ma et al., 2021a; Onel et al., 2014a; Onel et al., 2014b; Nielsen et al.,
78 2012; Da Silva, 2013). As a secondary amine, indole reaction with $\cdot\text{Cl}$ has the possibility of forming N-centered radicals and
79 subsequently forming nitrosamines via the reaction with NO. Since the -NH- group of indole is embedded in a unique chemical
80 environment compared to previously well-studied ONCs, the reaction mechanism of $\cdot\text{Cl}$ with indole remain elusive. In addition,
81 there are only a few studies concerning the reactions of polyfunctional heterocyclic ONCs with $\cdot\text{Cl}$.

82 In this work, we investigated the reaction mechanism and kinetics of indole initiated by $\cdot\text{OH}$ and $\cdot\text{Cl}$ by employing a
83 combination of quantum chemical calculations and kinetic modeling. The initial reactions of $\cdot\text{OH}/\cdot\text{Cl} + \text{indole}$ and the
84 subsequent reactions with O_2 of resulting intermediates were further investigated.

85 **2 Computational Details**

86 **2.1 Ab Initio Electronic Structure Calculations**

87 All the geometry optimizations and harmonic vibrational frequency calculations were performed at the M06-2X/6-
88 31+G(d,p) level of theory (Zhao and Truhlar, 2008). Intrinsic reaction coordinate calculations were performed to confirm the
89 connections of each transition state between the corresponding reactants and products. Single point energy calculations were
90 performed at the CBS-QB3 method based on the geometries at the M06-2X/6-31+G(d,p) level of theory (Montgomery et al.,
91 1999). The combination of the M06-2X functional and CBS-QB3 method has successfully been applied to predict radical-
92 molecule reactions (Guo et al., 2020; Ma et al., 2021b; Wang et al., 2018; Wang and Wang, 2016; Wu et al., 2015; Wang et al.,
93 2017; Fu et al., 2020). T_1 diagnostic (Table S2) values in the CCSD(T) calculations within the CBS-QB3 scheme for the
94 intermediates and transition states involved in the key reaction pathways were checked for multireference character. The T_1
95 diagnostic values for all checked important species in this work are lower than the threshold value of 0.045, indicating the

96 reliability of applied single reference methods (Rienstra-Kiracofe et al., 2000). In addition, similar to our previous studies, a
97 literature value of 0.8 kcal mol⁻¹ for the isolated ·Cl was used to account for the effect of spin-orbit coupling in the ·Cl + indole
98 reaction (Nicovich et al., 2015; Xie et al., 2017; Ma et al., 2018a). Atomic charges of indole and pre-reactive complexes in
99 the ·Cl + indole reaction are obtained by natural bond orbital (NBO) calculations (Reed et al., 1985). All calculations were
100 performed within the Gaussian 09 package (Frisch et al., 2009). Throughout the paper, the symbols “R, RC, PC, TS, IM and
101 P” stand for reactants, pre-reactive complexes, post-reactive complexes, transition states, intermediates and products involved
102 in the reactions, respectively, and their subscripts denote different species. In addition, “A//B” was used to present the
103 computational method, where “A” is the theoretical level for single point energy calculations and “B” is that for geometry
104 optimizations and harmonic frequency calculations.

105 **2.2 Kinetics Calculations**

106 MultiWell-2014.1 and MESMER 5.0 software were employed to investigate the kinetics for short time and long time
107 reaction, respectively (Barker and Ortiz, 2001; Barker, 2001; Glowacki et al., 2012). For the initial reactions of ·OH/·Cl +
108 indole, the reaction kinetics were calculated within the MultiWell-2014.1 program. For the subsequent reactions of resulting
109 primary intermediates, MESMER 5.0 were selected for simulating the reaction kinetics, since it has good performance for long
110 time runs, especially for simulating the variation of the different intermediates over time. Both MultiWell and MESMER codes
111 employ Rice-Ramsperger-Kassel-Marcus (RRKM) theory to calculate the reaction kinetics for reactions with intrinsic energy
112 barriers (Holbrook, 1996; Robinson, 1972). Long-range transition-state theory (LRTST) with a dispersion force potential
113 within the MultiWell-2014.1 program (Barker and Ortiz, 2001) or Inverse Laplace Transformation (ILT) method within the
114 MESMER 5.0 program was employed to calculate the reaction rate constants for the barrierless recombination reactions (from
115 R to RC and P to PC) (Rienstra-Kiracofe et al., 2000). Computational details for performing LRTST and ILT calculation were
116 described in our previous studies (Ma et al., 2021a; Ma et al., 2021b; Guo et al., 2020; Ding et al., 2020b). The parameters
117 used in the LRTST calculations and Lennard-Jones parameters of intermediates estimated by the empirical method proposed
118 by Gilbert and Smith (Gilbert, 1990) are listed in Table S3 and Table S4, respectively. N₂ was selected as the buffer gas, and
119 an average transfer energy of $\Delta E_d = 200$ cm⁻¹ was used to simulate the collision energy transfer between active intermediates
120 and N₂. In addition, ΔE_d between 50 - 250 cm⁻¹ were selected to study energy transfer parameters effects. For the reactions
121 involving H-abstraction or H-shift, tunneling effects were taken into account in all of the reaction rate constants calculations
122 by using a one-dimensional unsymmetrical Eckart barrier (Eckart, 1930), and were discussed in the Supporting Information
123 (SI). The kinetic calculations were primarily performed at 298 K and 1 atm, with additional ones at 0.1, 0.4 and 0.7 atm in the
124 troposphere relevant range to explore pressure effects. Variation of the energy transfer parameters and pressure resulted in
125 only minor changes (< 0.1%) in the calculated rate coefficients and branching ratios of main reaction pathways (see details in
126 the SI).

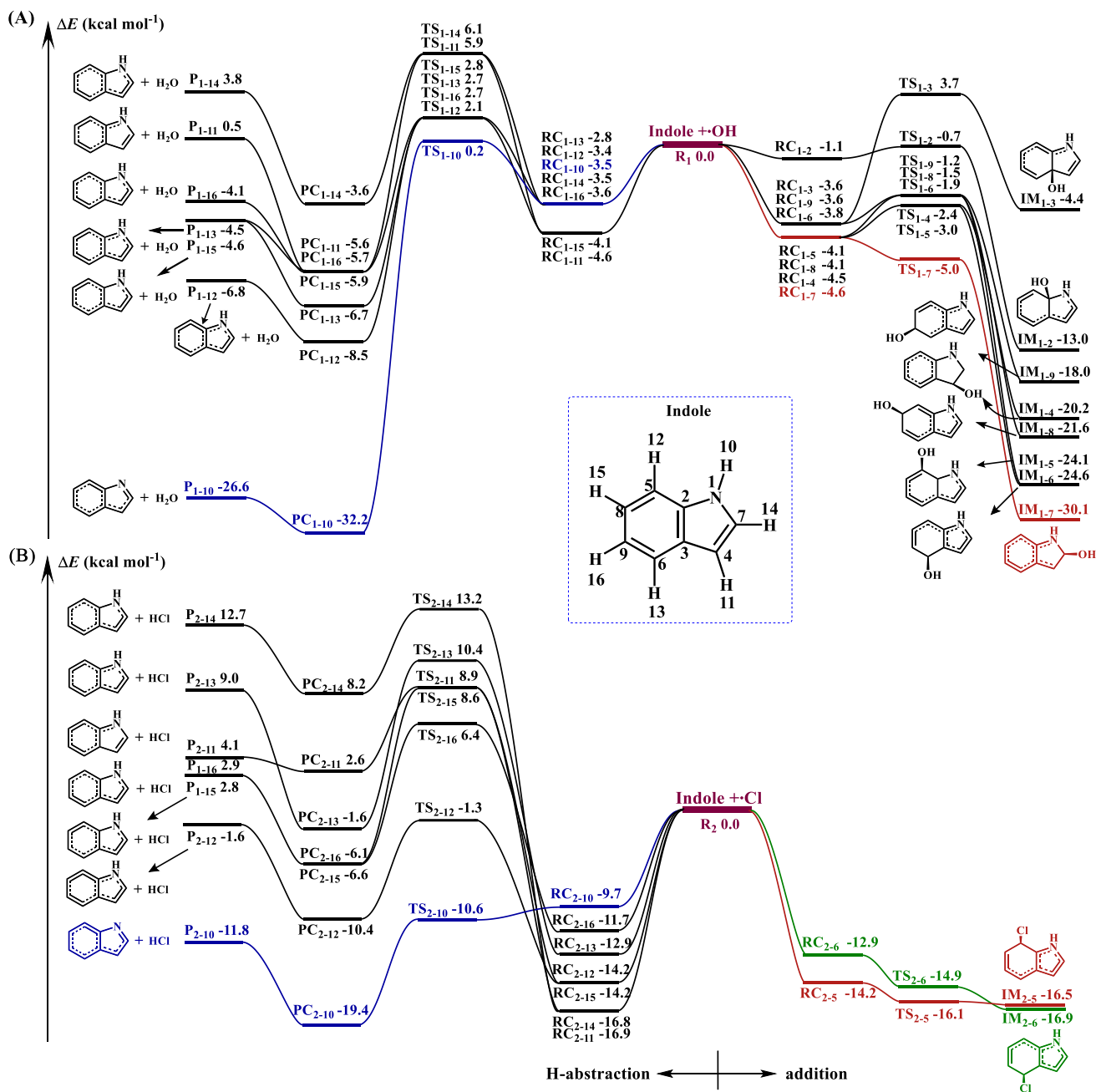
127 3 Results and Discussion

128 3.1 Initial Reactions of Indole

129 In principle, $\cdot\text{OH}$ and $\cdot\text{Cl}$ could add to the unsaturated $\text{C}=\text{C}$ bonds and benzene ring or directly abstract H-atoms connected
130 to either to a C-atom or the N-atom of indole. Considering the planar C_s structure of indole, $\cdot\text{OH}$ and $\cdot\text{Cl}$ addition to one side
131 of indole was only considered here. However, although numerous attempts have been made, we failed to locate the TSs and
132 addition IMs of $\cdot\text{Cl}$ addition to the C2, C3, C4, C7, C8 and C9 sites of indole (the numbering of the atoms is given in Figure
133 1), suggesting that such additions are in fact unfeasible. Therefore, 7 H-abstraction pathways of $\cdot\text{OH}$ and $\cdot\text{Cl}$, respectively,
134 8 $\cdot\text{OH}$ -addition pathways and 2 $\cdot\text{Cl}$ -addition pathways were considered for the $\cdot\text{OH}/\cdot\text{Cl}$ + indole reactions. The schematic
135 zero-point energy (ZPE) corrected potential energy surfaces of $\cdot\text{OH}/\cdot\text{Cl}$ + indole reactions are presented in Figure 1.

136 As can be seen from Figure 1, each H-abstraction reaction pathway proceeds through a RC and PC, and the addition
137 pathways through a RC for the $\cdot\text{OH}/\cdot\text{Cl}$ + indole reactions. For the H-abstraction pathways, the activation energy (E_a) for the
138 $-\text{NH}-$ group for both reactions are at least $2.0 \text{ kcal mol}^{-1}$ lower than the corresponding E_a values for the $-\text{CH}-$ groups. This
139 indicates that H-abstraction from the $-\text{NH}-$ group forming $\text{C}_8\text{H}_6\text{N}$ radicals and $\text{H}_2\text{O}/\text{HCl}$ is the most favorable among all the
140 H-abstraction pathways. In addition, the activation energy for the H-abstraction from the $-\text{NH}-$ group in the $\cdot\text{Cl}$ + indole
141 reaction is much lower than the corresponding $\cdot\text{OH}$ + indole reaction. This is consistent with previously reported reactions of
142 other amines with $\cdot\text{OH}$ and $\cdot\text{Cl}$ (Ma et al., 2018a; Ma et al., 2021a; Xie et al., 2014; Xie et al., 2015; Xie et al., 2017; Tan et
143 al., 2021; Ren and Da Silva, 2019; Borduas et al., 2015).

144 For the addition reactions, the most favorable reaction site differs for the indole + $\cdot\text{OH}$ and indole + $\cdot\text{Cl}$ reactions. Among
145 all 8 $\cdot\text{OH}$ addition pathways, $\cdot\text{OH}$ addition to the C7 site of the $\text{C}=\text{C}$ bond via $\text{TS}_{1,7}$ forming $\text{IM}_{1,7}$ is the most favorable
146 pathway. Different from the reaction with $\cdot\text{OH}$, the additions of $\cdot\text{Cl}$ to the C5 and C6 sites to form $\text{IM}_{2,5}$ and $\text{IM}_{2,6}$, respectively,
147 are significantly more favorable. By comparing the E_a values of the addition and H-abstraction pathways for both $\cdot\text{OH}/\cdot\text{Cl}$ +
148 indole reactions, it can be concluded that $\cdot\text{OH}$ addition to the C7 site is the most favorable for the $\cdot\text{OH}$ + indole reaction. All
149 the $\cdot\text{OH}$ + indole hydrogen abstraction reactions have high energy barriers. However, the additions of $\cdot\text{Cl}$ to the C5 and C6
150 sites as well as the $-\text{NH}-$ H-abstraction are all favorable due to their very lower E_a values for the $\cdot\text{Cl}$ + indole reaction.



151

152 **Figure 1: Schematic ZPE-corrected potential energy surface for the reactions of indole + ·OH (A) and indole + ·Cl (B)**
 153 **at the CBS-QB3//M062X/6-31+g(d,p) level of theory. The total energy of the reactants indole + ·OH/·Cl are set to zero,**
 154 **respectively (reference state).**

155

156

157

Interestingly, we found that all the pathways for the indole + ·Cl reaction can proceed via a stable 2c-3e bonded RC, which is different from that of the ·OH + indole reaction. Among all 2c-3e bonded RCs, only RC₂₋₁₀ from the -NH- abstraction pathway is formed between the N-atom and ·Cl, while the others are formed between the C-atom and ·Cl. Note that RC₂₋₁₁,

158 which forms from C-atom and $\cdot\text{Cl}$, is the most stable among all the formed RCs in the $\cdot\text{Cl}$ + indole reaction. To the best of our
 159 knowledge, this is the first time that such a stable 2c-3e bonded RC has been identified between the C-atom and $\cdot\text{Cl}$. In addition,
 160 the energy of RC₂₋₁₀ is higher than that of the traditional 2c-3e bonded RCs formed from alkylamine and $\cdot\text{Cl}$, which would
 161 result from the delocalization of lone pair electrons of the N-atom. By analyzing the NBO charges of these nine RCs (Table
 162 S5), we found that significant charge transfer occurs between $\cdot\text{Cl}$ and indole. The charge at Cl atom for RC₂₋₅, RC₂₋₆, RC₂₋₁₀,
 163 RC₂₋₁₁, RC₂₋₁₂, RC₂₋₁₃, RC₂₋₁₄, RC₂₋₁₅ and RC₂₋₁₆ are $-0.35 e$, $-0.33 e$, $-0.31 e$, $-0.39 e$, $-0.35 e$, $-0.33 e$, $-0.39 e$, $-0.35 e$ and $-$
 164 $0.33e$, respectively, indicating that all RCs are charge-transfer complexes. Similar charge-transfer complexes were also found
 165 in our previous study of the $\cdot\text{Cl}$ + piperazine reaction (Ma et al., 2018a).

166 With the master equation theory, the overall rate constants (k_{OH} and k_{Cl}) and branching ratios (Γ) for all H-abstraction and
 167 $\cdot\text{OH}/\cdot\text{Cl}$ -addition pathways involved in the $\cdot\text{OH}/\cdot\text{Cl}$ + indole reactions were calculated at 298 K and 1 atm. The calculated k_{OH}
 168 and k_{Cl} values of indole are $7.9 \times 10^{-11} \text{ cm}^3 \text{ molecule}^{-1} \text{ s}^{-1}$ and $2.9 \times 10^{-10} \text{ cm}^3 \text{ molecule}^{-1} \text{ s}^{-1}$, respectively. The calculated k_{OH}
 169 value is close to the available experimental value of $1.5 \times 10^{-10} \text{ cm}^3 \text{ molecule}^{-1} \text{ s}^{-1}$ (Atkinson et al., 1995), supporting the
 170 reliability of employed computational methods. Over the temperature range 230-330 K (Ma et al., 2018b), the calculated k_{OH}
 171 and k_{Cl} values have a negative correlation with temperature (Figure S1). Based on the calculated Γ values of the $\cdot\text{OH}/\cdot\text{Cl}$ +
 172 indole reactions (Table 1), it can be concluded that IM₁₋₇ (77%) is the main product for $\cdot\text{OH}$ + indole reaction, and IM₂₋₅ (31%),
 173 IM₂₋₆ (46%) and P₂₋₁₀ (C₈H₆N radicals + HCl) (23%) are the main products for $\cdot\text{Cl}$ + indole reaction. In addition, the calculated
 174 Γ values of IM₁₋₇, IM₂₋₅, IM₂₋₆ and P₂₋₁₀ (C₈H₆N radicals + HCl) change negligibly with the variation of temperature, pressure
 175 and energy transfer parameters (SI). Therefore, we mainly considered the further transformation of IM₁₋₇, IM₂₋₅, IM₂₋₆ and
 176 C₈H₆N radicals in the following part.

177 **Table 1. Calculated branching ratios (Γ) for the indole + $\cdot\text{OH}/\cdot\text{Cl}$ reactions at 298 K and 1 atm.**

Pathways	Species	Γ	Species	Γ	Species	Γ
$\cdot\text{OH}$ + Indole	IM ₁₋₂	0	IM ₁₋₃	0	IM ₁₋₄	5%
	IM ₁₋₅	12%	IM ₁₋₆	3%	IM ₁₋₇	77%
	IM ₁₋₈	1%	IM ₁₋₉	1%	P ₁₋₁₀	1%
	P ₁₋₁₁	0	P ₁₋₁₂	0	P ₁₋₁₃	0
	P ₁₋₁₄	0	P ₁₋₁₅	0	P ₁₋₁₆	0
$\cdot\text{Cl}$ + Indole	IM ₂₋₅	31%	IM ₂₋₆	46%	P ₂₋₁₀	23%
	P ₂₋₁₁	0	P ₂₋₁₂	0	P ₂₋₁₃	0
	P ₂₋₁₄	0	P ₂₋₁₅	0	P ₂₋₁₆	0

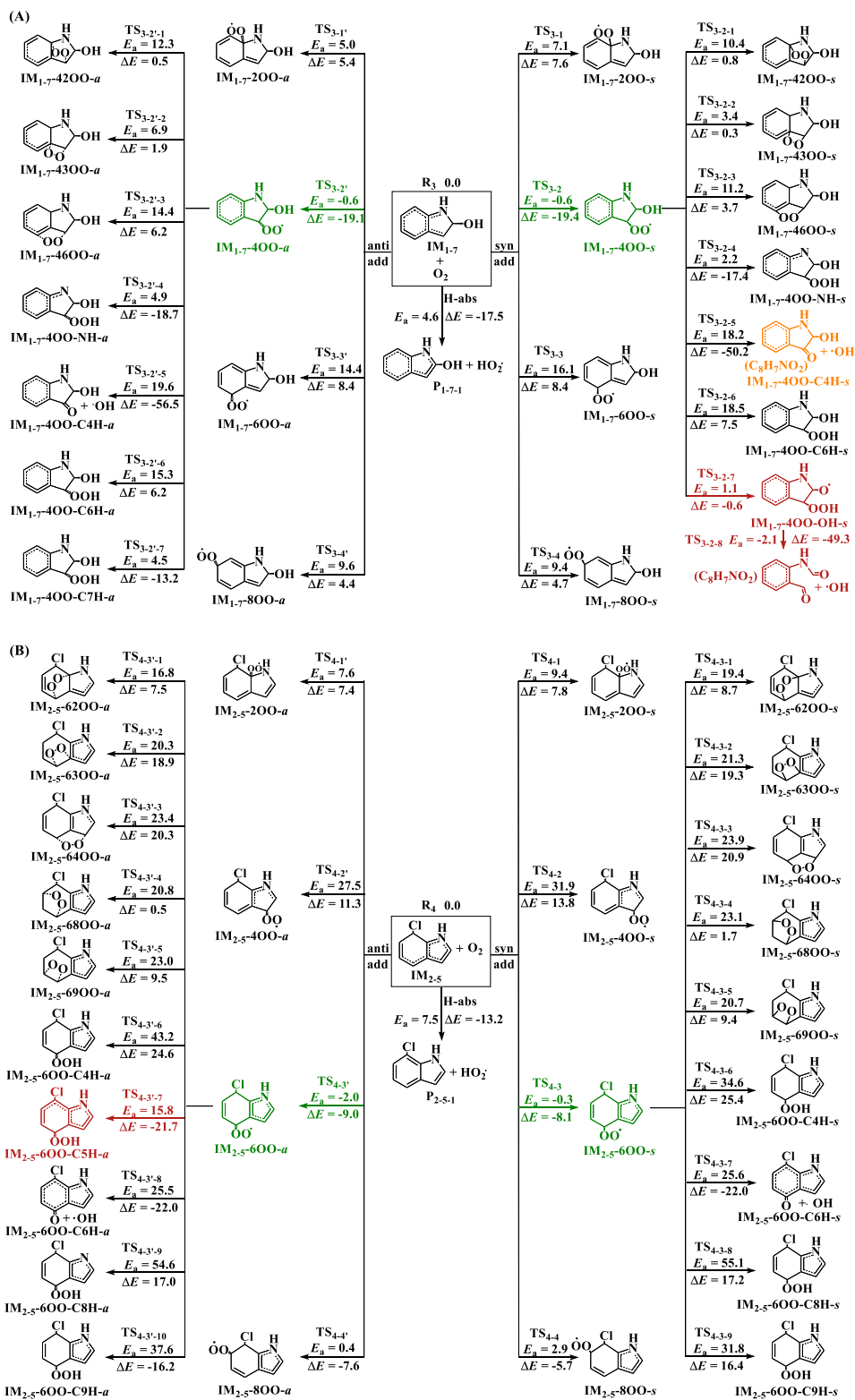
178 3.2 Subsequent Reactions of Addition Intermediates

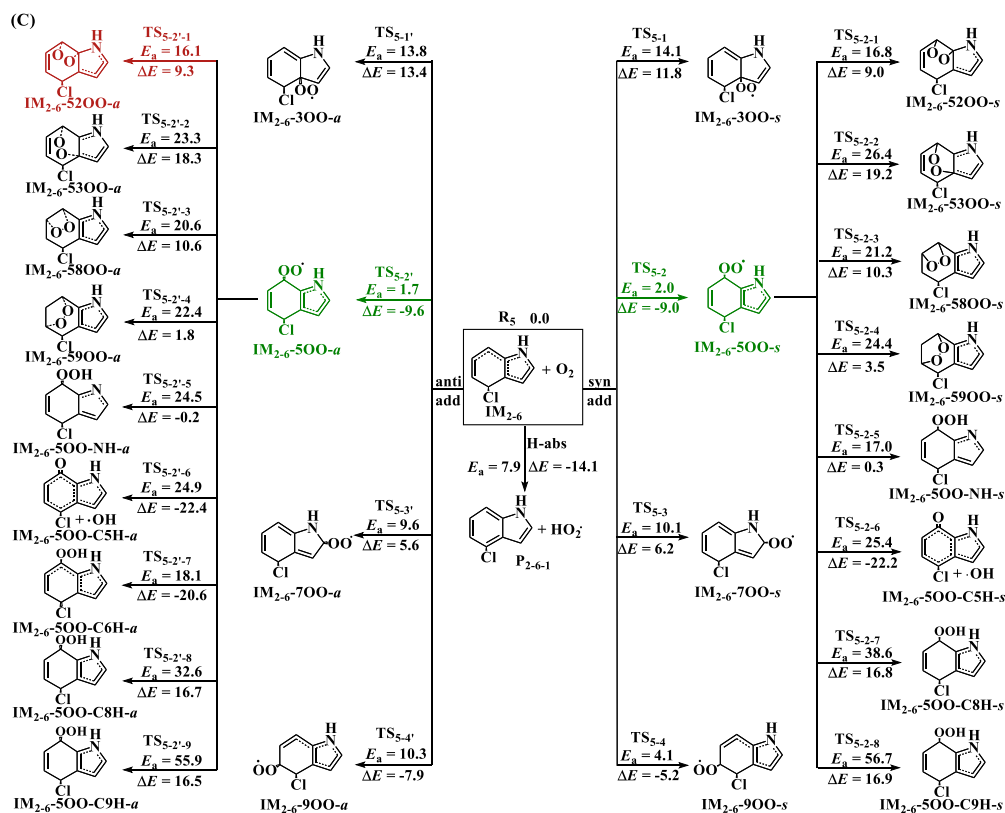
179 Similar to other C-centered radicals (Zhang et al., 2012; Guo et al., 2020; Ma et al., 2021b; Yu et al., 2016; Yu et al., 2017;
 180 Ji et al., 2017; Ding et al., 2020a), the intermediates IM₁₋₇, IM₂₋₅ and IM₂₋₆ will subsequently react with O₂. Two different

181 pathways (Figure 2) were considered for the reactions of the intermediates IM_{1-7} , IM_{2-5} and IM_{2-6} with O_2 . One is the direct
182 hydrogen abstraction by O_2 from the C site connecting to the -OH or -Cl group forming P_{1-7-1} ($C_8H_7NO + HO_2\cdot$), P_{2-5-1} (C_8H_6NCl
183 + $HO_2\cdot$) and P_{2-6-1} ($C_8H_6NCl + HO_2\cdot$). The other is the O_2 addition to the C sites with high spin density (see spin density
184 distribution in Table S10) of the intermediates IM_{1-7} , IM_{2-5} and IM_{2-6} to form peroxy radicals $Q-iOO-a/s$, where Q stands for
185 intermediates IM_{1-7} , IM_{2-5} and IM_{2-6} , i stands for the numbering of the C-positions where O_2 is added. The O_2 molecule can be
186 added to the same (-syn, abbreviated as -s) and opposite (-anti, abbreviated as -a) sides of the plane relative to -OH or -Cl
187 group. The C2, C4, C6 and C8 sites of IM_{1-7} , C2, C4, C6 and C8 sites of IM_{2-5} and C3, C5, C7 and C9 sites of IM_{2-6} are high
188 spin density sites susceptible for O_2 addition.

189 As can be seen from the energetic data shown in Figure 2, O_2 addition to the C4 site of IM_{1-7} to form $IM_{1-7-4OO-a/s}$ (-
190 0.6/-0.6 kcal mol⁻¹), C6 site of IM_{2-5} to form $IM_{2-5-6OO-a/s}$ (-0.3/-2.0 kcal mol⁻¹) and C5 site of IM_{2-6} to form $IM_{2-6-5OO-a/s}$
191 (2.0/1.7 kcal mol⁻¹) are the most favorable among all possible entrance pathways for the respective reactions. It deserves
192 mentioning that the formation energy (ΔE) of $IM_{2-5-6OO-a/s}$ and $IM_{2-6-5OO-a/s}$ are only about 9.0 kcal mol⁻¹, which could
193 indicate that they likely re-dissociate back to the reactants IM_{2-5}/IM_{2-6} and O_2 , if $IM_{2-5-6OO-a/s}$ and $IM_{2-6-5OO-a/s}$ does not
194 rapidly transform to other species.

195 For the further transformation of the formed peroxy radicals $IM_{1-7-4OO(-a/s)}$, $IM_{2-5-6OO(-a/s)}$ and $IM_{2-6-5OO(-a/s)}$, two
196 transformation pathways were identified. The first is cyclization reactions where the terminal O-atom of -OO attacks the
197 different C-positions to form bicycle radicals $Q-ijOO(-a/s)$ (j stands the number of the C-positions attacked by terminal O-
198 atom). The second is H-shifts from -OH, -NH- and different -CH- sites to the terminal O-atom to form various hydroperoxide
199 radicals $Q-iOO-OH(-a/s)$, $Q-iOO-NH(-a/s)$ and $Q-iOO-CkH(-a/s)$ (k stands the number of the C-positions from which H is
200 shifted), respectively. For $IM_{1-7-4OO(-a/s)}$ and $IM_{2-5-6OO(-a/s)}$, forming $IM_{1-7-4OO-OH-s}$ and $IM_{2-5-6OO-C5H-a}$ via H-shift
201 reactions are the most favorable, respectively. However, for $IM_{2-6-5OO(-a/s)}$, the cyclization reaction forming $IM_{2-6-52OO-a}$
202 is the most favorable. It is noted that the formed $IM_{1-7-4OO-OH-s}$ from $IM_{1-7-4OO(-a/s)}$ can barrierlessly transform to form
203 $C_8H_7NO_2$ (N-(2-formylphenyl)formamide) and $\cdot OH$ (collectively denoted $P_{1-7-4-1}$) via concerted C-C and O-O bonds rupture.
204 The further transformation of the peroxy radicals $IM_{1-7-4OO(-a/s)}$, $IM_{2-5-6OO(-a/s)}$ and $IM_{2-6-5OO(-a/s)}$ need to overcome
205 barriers above 20.5 kcal mol⁻¹ (relative to their respective peroxy radicals), indicating that the further transformation of IM_{1-7-}
206 $4OO(-a/s)$, $IM_{2-5-6OO(-a/s)}$ and $IM_{2-6-5OO(-a/s)}$ should be very slow.

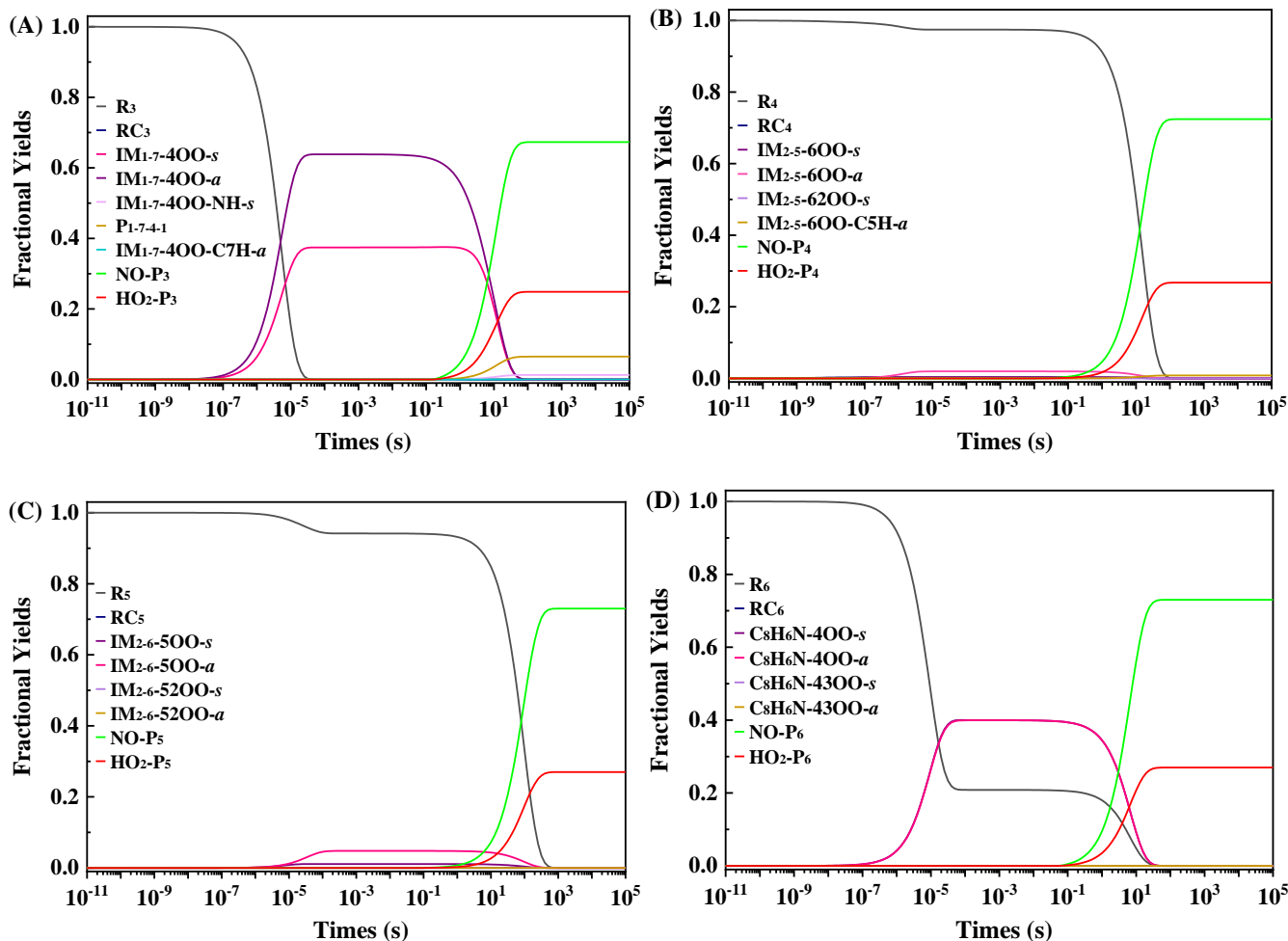




209

210 **Figure 2: Reaction pathways and corresponding energetic data for the reactions of IM₁₋₇ (A), IM₂₋₅ (B) and IM₂₋₆ (C)**
 211 **with O₂. Units are in kcal mol⁻¹.**

212 Based on the energetic data of the favorable reaction pathways, MESMER modeling was employed to investigate the
 213 reaction rate constants and fractional yields for the reactions of IM₁₋₇, IM₂₋₅, and IM₂₋₆ with O₂. Similar to previous studies
 214 (Guo et al., 2020; Ma et al., 2021a; Ma et al., 2021b; Zhang et al., 2012; Fu et al., 2020), bimolecular reactions with NO/HO₂-
 215 are considered as competitive pathways for the unimolecular reactions of the peroxy radicals IM₁₋₇-4OO(-a/s), IM₂₋₅-6OO(-
 216 a/s) and IM₂₋₆-5OO(-a/s) by simply adding their pseudo-first-order rate constants into the master equation modeling. Here,
 217 applied pseudo first order rate constants for peroxy radicals (IM₁₋₇-4OO(-a/s), IM₂₋₅-6OO(-a/s) and IM₂₋₆-5OO(-a/s)) reaction
 218 with NO and HO₂· are 0.06 s⁻¹ and 0.02 s⁻¹, respectively, corresponding to reactions occurring at 200 ppt NO and 50 ppt
 219 HO₂· conditions (Hofzumahaus et al., 2009; Yu et al., 2020; Praske et al., 2018). The reactions of peroxy radicals with NO and
 220 HO₂· should form organonitrate/alkoxy radicals (collectively denoted NO-P_n, where *n* marks products from the different
 221 peroxy radical reactions) and hydroperoxide (HO₂-P_n), respectively. Pseudo-first-order rate constants of IM₁₋₇, IM₂₋₅, and IM₂₋₆
 222 with O₂ are calculated to be 3.0 × 10⁷ s⁻¹, based on the reaction rate constants of IM₁₋₇, IM₂₋₅, and IM₂₋₆ with O₂ (6.0 × 10⁻¹²
 223 cm³ molecule⁻¹ s⁻¹) and the concentration of O₂ ([O₂] = 5.0 × 10¹⁸ molecule cm⁻³). The simulated time-dependent fractional
 224 yields are presented in Figure 3.



225

226

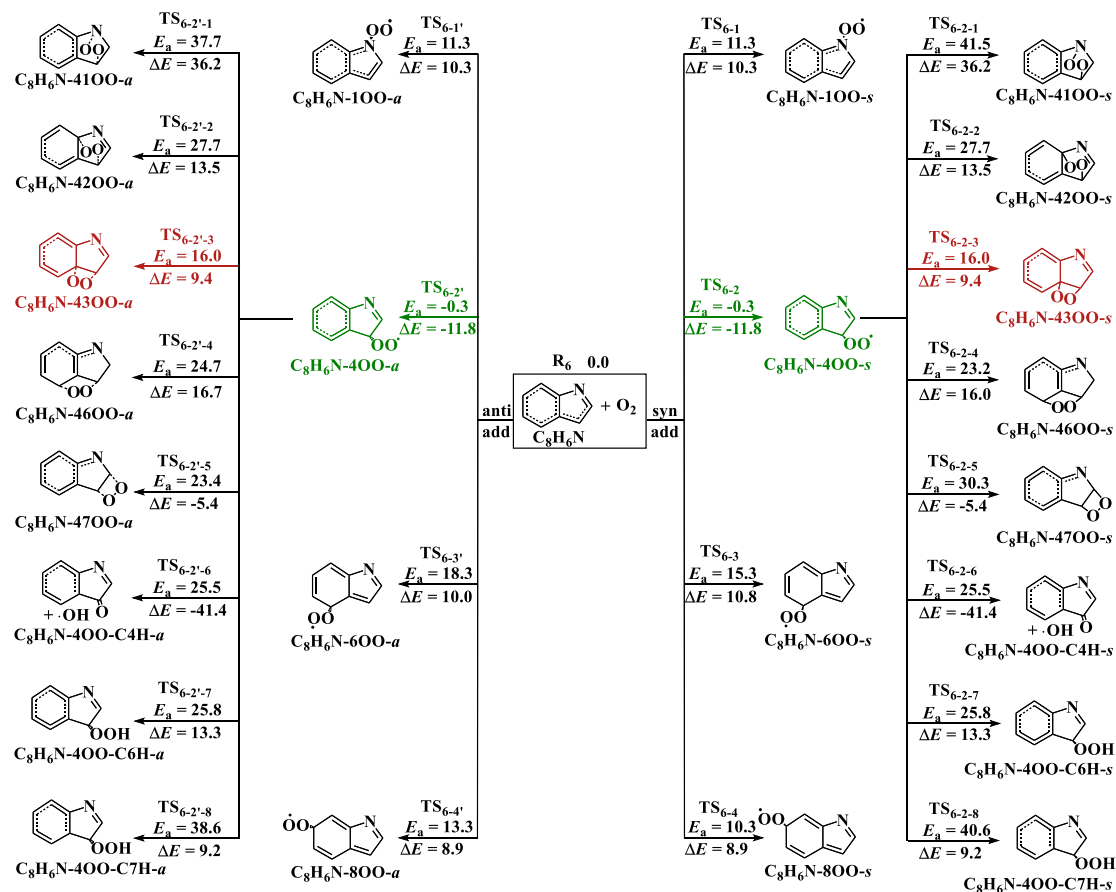
227 **Figure 3: Calculated fractional yields of species (at 200 ppt NO and 50 ppt HO₂· conditions) as a function of time in the**
 228 **reactions of IM₁₋₇ (A), IM₂₋₅ (B), IM₂₋₆ (C) and C₈H₆N (D) with O₂ at 298 K and 1 atm.**

229 As can be seen in Figure 3, after 100 s, the reactions of IM₁₋₇, IM₂₋₅ and IM₂₋₆ with O₂ mainly form the organonitrate/alkoxy
 230 radicals NO-P₃ (C₈H₈N₂O₃/C₈H₈NO₂·), NO-P₄ (C₈H₇N₂O₃Cl/C₈H₇NCIO·) and NO-P₅ (C₈H₇N₂O₃Cl/C₈H₇NCIO·), followed by
 231 the formation of hydroperoxide HO₂-P₃ (C₈H₉NO₃), HO₂-P₄ (C₈H₈NO₂Cl) and HO₂-P₅ (C₈H₈NO₂Cl), respectively. For the
 232 reactions of IM₂₋₅ and IM₂₋₆ with O₂, the main products formed are NO-P_{4/5} and HO₂-P_{4/5}. In contrast, the IM₁₋₇ + O₂ reaction
 233 also lead to the fragmental products P₁₋₇₋₄₋₁ (C₈H₇NO₂ and ·OH) besides the main products NO-P₃ and HO₂-P₃. This difference
 234 in product branching ratios results from the lower unimolecular reaction energy barrier of the peroxy radicals IM₁₋₇-4OO(-a/s)
 235 from the reaction of IM₁₋₇ with O₂ than those of IM₂₋₅-6OO(-a/s) and IM₂₋₆-5OO(-a/s) from the reactions of IM₂₋₅ and IM₂₋₆
 236 with O₂. It should be noted that the C₈H₇NO₂ product has been detected in previous experimental study of the ·OH + indole
 237 reaction (Montoya-Aguilera et al., 2017), supporting the validity of our computational results.

238 An obvious difference for these three reactions is that the reaction of IM₁₋₇ with O₂ can form peroxy radicals IM₁₋₇-4OO(-
239 *a/s*) with high yields during the reactions. However, the yields of the corresponding peroxy radicals IM₂₋₅-6OO(-*a/s*) and IM₂₋₆-
240 5OO(-*a/s*) from the reactions of IM₂₋₅ and IM₂₋₆ with O₂ are low. The difference mainly originates from the difference in the
241 formation energy of these three peroxy radicals as shown in Figure 2. The ΔE values of IM₁₋₇-4OO(-*a/s*)(-19.1/-19.4 kcal mol⁻¹)
242 are much more lower than those of IM₂₋₅-6OO(-*a/s*)(-9.0/-8.1 kcal mol⁻¹) and IM₂₋₆-5OO(-*a/s*)(-9.6/-9.0 kcal mol⁻¹). As
243 discussed above, the high formation energy of IM₂₋₅-6OO(-*a/s*) and IM₂₋₆-5OO(-*a/s*) should make IM₂₋₅-6OO(-*a/s*) and IM₂₋₆-
244 5OO(-*a/s*) return back to the reactants, explaining the reason for the lower yields of IM₂₋₅-6OO(-*a/s*) and IM₂₋₆-5OO(-*a/s*).

245 3.3 Subsequent Reactions of C₈H₆N radicals from the H-abstraction pathway

246 Here, the bimolecular reaction with O₂ was mainly considered for C₈H₆N radicals as its sole atmospheric fate. It was
247 found that the spin density distribution was mainly centered at the C atoms (C4 (0.662), C6 (0.261), C8 (0.178)) and N atom
248 (0.256), indicating that the C₈H₆N radical is delocalized. This is in contrast to previously studied N-centered radicals formed
249 from alkylamines oxidation, which are highly localized (Xie et al., 2015; Xie et al., 2014; Ma et al., 2018a; Tan et al., 2021;
250 Borduas et al., 2015). Therefore, O₂ addition to the C4, C6, C8 and N1 sites (including attack from both sides) are considered
251 for the reaction of the C₈H₆N radicals with O₂. As can be seen from Figure 4, O₂ additions to the C4 site of the C₈H₆N radicals
252 forming C₈H₆N-4OO-*a/s* with E_a of -0.3 kcal mol⁻¹ are the most favorable, translating to pseudo-first-order reaction rate
253 constants of 3.0×10^7 s⁻¹. Such rate constants are about 7 orders of magnitude higher than that of typical N-centered radicals
254 reacting with NO even under very high NO concentration (5 ppb). Therefore, C₈H₆N radicals does not react with NO to form
255 carcinogenic nitrosamines in any appreciable amount, which is different from the previously reported reaction mechanism of
256 N-centered radicals formed from the reactions of alkylamines with ·Cl (Xie et al., 2015; Xie et al., 2014; Ma et al., 2018a). To
257 the best of our knowledge, this is the first study to reveal that despite forming radicals by abstracting an H-atom at the N-site,
258 carcinogenic nitrosamines were not produced in the indole oxidation reaction.



259

260 **Figure 4: Reaction pathways and corresponding energetic data for the reactions of C_8H_6N radicals with O_2 . Units are**
 261 **in kcal mol^{-1} .**

262 For the transformation of the formed $C_8H_6N-400-a/s$ radicals, the ring closure reaction to form $C_8H_6N-4300-a/s$ is the
 263 most favorable, but still needs to overcome a $27.8 \text{ kcal mol}^{-1}$ energy barrier, therefore the further transformation of the formed
 264 $C_8H_6N-400-a/s$ should proceed very slowly. The $C_8H_6N-400-a/s$ should mainly react with NO and $HO_2\cdot$ to form $NO-P_6$ and
 265 HO_2-P_6 . Detailed kinetics calculations (Figure 3D) further confirm that the reaction of C_8H_6N radicals with O_2 mainly form
 266 $NO-P_6$ and HO_2-P_6 under 200 ppt NO and 50 ppt $HO_2\cdot$ conditions.

267 4 Comparison with Available Experimental Results and Atmospheric Implications.

268 This study found that $\cdot OH/\cdot Cl$ initiated reactions of indole mainly form organonitrates, alkoxy radicals and hydroperoxide
 269 products with N -(2-formylphenyl)formamide ($C_8H_7NO_2$) as a minor product at 200 ppt NO and 50 ppt $HO_2\cdot$ conditions. The
 270 formed closed-shell products have high oxygen-to-carbon ratios compared to indole and therefore are expected to have lower
 271 vapor pressures, likely being first generation products that can be further oxidized and contribute to the formation of SOA.

272 With our findings, a comparison was made with the available experimental study on $\cdot\text{OH}$ initiated reaction of indole. The
273 calculated k_{OH} values ($7.9 \times 10^{-11} \text{ cm}^3 \text{ molecule}^{-1} \text{ s}^{-1}$) of indole is consistent with the experimental value ($15 \times 10^{-11} \text{ cm}^3$
274 $\text{molecule}^{-1} \text{ s}^{-1}$) (Atkinson et al., 1995), indicating the reliability of applied theoretical methods. A signal with the molecular
275 formula $\text{C}_8\text{H}_7\text{NO}_2$ has been observed in the mass spectrum in an experimental study (Montoya-Aguilera et al., 2017),
276 supporting the formation of the predicted N-(2-formylphenyl)formamide. To the best of our knowledge, this study is the first
277 to reveal that the chemical identity of the mass spectrum signal as N-(2-formylphenyl)formamide, as opposed to the proposed
278 3-oxy-2-hydroxy-indole. In addition, monomeric products (isatin and isatoic anhydride) and dimer products has not been
279 observed in our computational study. We speculate that they may be produced from the subsequent conversion of the formed
280 alkoxy radicals, multi-generation reactions of organonitrates and hydroperoxide and self/cross reactions of peroxy radicals
281 ($\text{RO}_2 + \text{RO}_2$). Therefore, further studies are warranted to investigate the subsequent transformation of the formed alkoxy
282 radicals, organonitrates and hydroperoxide, and the $\text{RO}_2 + \text{RO}_2$ reactions, to accurately describe the atmospheric impact of
283 indole.

284 The calculated k_{Cl} value of the indole + $\cdot\text{Cl}$ reaction is a factor of 3.7 higher than that of the indole + $\cdot\text{OH}$ reaction, and is
285 close to the k_{Cl} values for the reactions of alkylamines, heterocyclic amines and amides with $\cdot\text{Cl}$ (Xie et al., 2017; Xie et al.,
286 2015; Ma et al., 2018a; Nicovich et al., 2015). The contribution of $\cdot\text{Cl}$ to the transformation of indole is calculated to be 3.6-
287 36% that of $\cdot\text{OH}$, assuming $\cdot\text{Cl}$ concentrations equal to 1-10% of that of $\cdot\text{OH}$ (Wang and Ruiz, 2017; Nicovich et al., 2015;
288 Xie et al., 2017; Xie et al., 2015; Ma et al., 2018a). Therefore, $\cdot\text{Cl}$ plays an important role in the overall transformation of
289 indole. More importantly, $\cdot\text{Cl}$ initiated reaction of indole does not lead to the formation of carcinogenic nitrosamines although
290 $\cdot\text{Cl}$ can favorably abstract the H-atom from N-site to form $\text{C}_8\text{H}_6\text{N}$ radicals, which is a plausible precursor of carcinogenic
291 nitrosamines. Hence, to the best of our knowledge, this is the first study to reveal that despite forming radicals by abstracting
292 an H-atom at the N-site, carcinogenic nitrosamines were not produced in the indole oxidation reaction. This is most likely
293 caused by the delocalized character of the formed $\text{C}_8\text{H}_6\text{N}$ radicals due to the existence of the adjacent unsaturated bonds.
294 Therefore, this study further confirm that the functional groups connected to the NH_x ($x = 1, 2$) group highly affect the
295 atmospheric fate of ONCs. Further studies should be performed to investigate the structure-activity relationship of $\cdot\text{Cl}$ initiated
296 reactions of ONCs to comprehensively evaluate their atmospheric impacts.

297

298 *Data availability.* The data in this article are available from the corresponding author upon request (maff@dlut.edu.cn,
299 hbxie@dlut.edu.cn).

300 *Author contribution.* FFM and HBX designed research; JWX, FFM and HBX performed research; JWX, FFM and HBX
301 analyzed data; JWX, FFM, JE, HBX and JWC wrote the paper; and FFM, HBX, JE and JWC reviewed and revised the paper.

302 *Competing interests.* The authors declare that they have no conflict of interest.

303 *Acknowledgements.* We thank Dr. Struan H. Robertson (Dassault Systèmes) for the discussion on the MESMER simulations.
304 The study was supported by the LiaoNing Revitalization Talents Program (XLYC1907194), National Natural Science
305 Foundation of China (21876024), the Major International (Regional) Joint Research Project (21661142001) and
306 Supercomputing Center of Dalian University of Technology.

307 **References**

- 308 Almeida, J., Schobesberger, S., Kürten, A., Ortega, I. K., Kupiainen-Määttä, O., Praplan, A. P., Adamov, A., Amorim, A.,
309 Bianchi, F., Breitenlechner, M., David, A., Dommen, J., Donahue, N. M., Downard, A., Dunne, E., Duplissy, J., Ehrhart, S.,
310 Flagan, R. C., Franchin, A., Guida, R., Hakala, J., Hansel, A., Heinritzi, M., Henschel, H., Jokinen, T., Junninen, H., Kajos,
311 M., Kangasluoma, J., Keskinen, H., Kupc, A., Kurtén, T., Kvashin, A. N., Laaksonen, A., Lehtipalo, K., Leiminger, M., Leppä,
312 J., Loukonen, V., Makhmutov, V., Mathot, S., McGrath, M. J., Nieminen, T., Olenius, T., Onnela, A., Petäjä, T., Riccobono,
313 F., Riipinen, I., Rissanen, M., Rondo, L., Ruuskanen, T., Santos, F. D., Sarnela, N., Schallhart, S., Schnitzhofer, R., Seinfeld,
314 J. H., Simon, M., Sipilä, M., Stozhkov, Y., Stratmann, F., Tomé, A., Tröstl, J., Tsagkogeorgas, G., Vaattovaara, P., Viisanen,
315 Y., Virtanen, A., Vrtala, A., Wagner, P. E., Weingartner, E., Wex, H., Williamson, C., Wimmer, D., Ye, P., Yli-Juuti, T.,
316 Carslaw, K. S., Kulmala, M., Curtius, J., Baltensperger, U., Worsnop, D. R., Vehkamäki, H., and Kirkby, J.: Molecular
317 understanding of sulphuric acid-amine particle nucleation in the atmosphere, *Nature*, 502, 359-363,
318 <https://doi.org/10.1038/nature12663>, 2013.
- 319 Atkinson, R., Tuazon, E. C., Arey, J., and Aschmann, S. M.: Atmospheric and indoor chemistry of gas-phase indole, quinoline,
320 and isoquinoline, *Atmos. Environ.*, 29, 3423-3432, [https://doi.org/10.1016/1352-2310\(95\)00103-6](https://doi.org/10.1016/1352-2310(95)00103-6), 1995.
- 321 Atkinson, R., Baulch, D. L., Cox, R. A., Hampson, R. F., Kerr, J. A., and Troe, J.: Evaluated Kinetic and Photochemical Data
322 for Atmospheric Chemistry: Supplement III. IUPAC Subcommittee on Gas Kinetic Data Evaluation for Atmospheric
323 Chemistry, *J. Phys. Chem. Ref. Data*, 18, 881-1097, <https://doi.org/10.1063/1.555832>, 1989.
- 324 Barker, J. R.: Multiple-well, multiple-path unimolecular reaction systems. I. MultiWell computer program suite, *Int. J. Chem.*
325 *Kinet.*, 33, 232-245, <https://doi.org/10.1002/kin.1017>, 2001.
- 326 Barker, J. R. and Ortiz, N. F.: Multiple-Well, multiple-path unimolecular reaction systems. II. 2-methylhexyl free radicals, *Int.*
327 *J. Chem. Kinet.*, 33, 246-261, <https://doi.org/10.1002/kin.1018>, 2001.
- 328 Borduas, N., da Silva, G., Murphy, J. G., and Abbatt, J. P. D.: Experimental and Theoretical Understanding of the Gas Phase
329 Oxidation of Atmospheric Amides with OH Radicals: Kinetics, Products, and Mechanisms, *J. Phys. Chem. A*, 119, 4298-4308,
330 <https://doi.org/10.1021/jp503759f>, 2015.
- 331 Borduas, N., Abbatt, J. P. D., Murphy, J. G., So, S., and da Silva, G.: Gas-Phase Mechanisms of the Reactions of Reduced
332 Organic Nitrogen Compounds with OH Radicals, *Environ. Sci. Technol.*, 50, 11723-11734,
333 <https://doi.org/10.1021/acs.est.6b03797>, 2016.

334 Borduas, N., Murphy, J. G., Wang, C., da Silva, G., and Abbatt, J. P. D.: Gas Phase Oxidation of Nicotine by OH Radicals:
335 Kinetics, Mechanisms, and Formation of HNCO, *Environ. Sci. Technol. Lett.*, 3, 327-331,
336 <https://doi.org/10.1021/acs.estlett.6b00231>, 2016.

337 Bunkan, A. J. C., Mikoviny, T., Nielsen, C. J., Wisthaler, A., and Zhu, L.: Experimental and Theoretical Study of the OH-
338 Initiated Photo-oxidation of Formamide, *J. Phys. Chem. A*, 120, 1222-1230, <https://doi.org/10.1021/acs.jpca.6b00032>, 2016.

339 Bunkan, A. J. C., Hetzler, J., Mikoviny, T., Wisthaler, A., Nielsen, C. J., and Olzmann, M.: The reactions of N-
340 methylformamide and N,N-dimethylformamide with OH and their photo-oxidation under atmospheric conditions:
341 experimental and theoretical studies, *Phys. Chem. Chem. Phys.*, 17, 7046-7059, <https://doi.org/10.1039/C4CP05805D>, 2015.

342 Cardoza, Y. J., Lait, C. G., Schmelz, E. A., Huang, J., and Tumlinson, J. H.: Fungus-Induced Biochemical Changes in Peanut
343 Plants and Their Effect on Development of Beet Armyworm, *Spodoptera Exigua* Hübner (Lepidoptera: Noctuidae) Larvae,
344 *Environ. Entomol.*, 32, 220-228, <https://doi.org/10.1603/0046-225X-32.1.220>, 2003.

345 Chen, J., Jiang, S., Liu, Y.-R., Huang, T., Wang, C. Y., Miao, S. K., Wang, Z. Q., Zhang, Y., and Huang, W.: Interaction of
346 oxalic acid with dimethylamine and its atmospheric implications, *RSC Adv.*, 7, 6374-6388,
347 <https://doi.org/10.1039/C6RA27945G>, 2017.

348 Crounse, J. D., Nielsen, L. B., Jørgensen, S., Kjaergaard, H. G., and Wennberg, P. O.: Autoxidation of Organic Compounds
349 in the Atmosphere, *J. Phys. Chem. Lett.*, 4, 3513-3520, <https://doi.org/10.1021/jz4019207>, 2013.

350 Ding, Z., Yi, Y., Wang, W., and Zhang, Q.: Atmospheric oxidation of indene initiated by OH radical in the presence of O₂ and
351 NO: A mechanistic and kinetic study, *Chemosphere*, 259, 127331, <https://doi.org/10.1016/j.chemosphere.2020.127331>, 2020a.

352 Ding, Z., Yi, Y., Wang, W., and Zhang, Q.: Understanding the role of Cl and NO₃ radicals in initiating atmospheric oxidation
353 of fluorene: A mechanistic and kinetic study, *Sci. Total Environ.*, 716, 136905,
354 <https://doi.org/10.1016/j.scitotenv.2020.136905>, 2020b.

355 da Silva, G.: Formation of Nitrosamines and Alkyldiazohydroxides in the Gas Phase: The CH₃NH + NO Reaction Revisited,
356 *Environ. Sci. Technol.*, 47, 7766-7772, <https://doi.org/10.1021/es401591n>, 2013.

357 Eckart, C.: The penetration of a potential barrier by electrons, *Phys. Rev.*, 35, 1303-1309,
358 <https://doi.org/10.1103/PhysRev.35.1303>, 1930.

359 Ehn, M., Thornton, J. A., Kleist, E., Sipilä, M., Junninen, H., Pullinen, I., Springer, M., Rubach, F., Tillmann, R., Lee, B.,
360 Lopez-Hilfiker, F., Andres, S., Acir, I.-H., Rissanen, M., Jokinen, T., Schobesberger, S., Kangasluoma, J., Kontkanen, J.,
361 Nieminen, T., Kurtén, T., Nielsen, L. B., Jørgensen, S., Kjaergaard, H. G., Canagaratna, M., Maso, M. D., Berndt, T., Petäjä,
362 T., Wahner, A., Kerminen, V.-M., Kulmala, M., Worsnop, D. R., Wildt, J., and Mentel, T. F.: A large source of low-volatility
363 secondary organic aerosol, *Nature*, 506, 476-479, <https://doi.org/10.1038/nature13032>, 2014.

364 Faxon, C. B. and Allen, D. T.: Chlorine chemistry in urban atmospheres: a review, *Environ. Chem.*, 10, 221-233,
365 <https://doi.org/10.1071/en13026>, 2013.

366 Fu, Z., Xie, H. B., Elm, J., Guo, X., Fu, Z., and Chen, J.: Formation of Low-Volatile Products and Unexpected High
367 Formaldehyde Yield from the Atmospheric Oxidation of Methylsiloxanes, *Environ. Sci. Technol.*, 54, 7136-7145,
368 <https://doi.org/10.1021/acs.est.0c01090>, 2020.

369 Frisch, M. J., Trucks, G. W., Schlegel, H. B., Scuseria, G. E., Robb, M. A., Cheeseman, J. R., Scalmani, G., Barone, V.,
370 Mennucci, B., Petersson, G. A., Nakatsuji, H., Caricato, M., Li, X., Hratchian, H. P., Izmaylov, A. F., Bloino, J., Zheng, G.,
371 Sonnenberg, J. L., Hada, M., Ehara, M., Toyota, K., Fukuda, R., Hasegawa, J., Ishida, M., Nakajima, T., Honda, Y., Kitao, O.,
372 Nakai, H., Vreven, T., Montgomery, J. A., Jr, Peralta, J. E., Ogliaro, F., Bearpark, M., Heyd, J. J., Brothers, E., Kudin, K. N.,
373 Staroverov, V. N., Kobayashi, R., Normand, J., Raghavachari, K., Rendell, A., Burant, J. C., Iyengar, S. S., Tomasi, J., Cossi,
374 M., Rega, N., Millam, J. M., Klene, M., Knox, J. E., Cross, J. B., Bakken, V., Adamo, C., Jaramillo, J., Gomperts, R., Stratmann,
375 R. E., Yazyev, O., Austin, A. J., Cammi, R., Pomelli, C., Ochterski, J. W., Martin, R. L., Morokuma, K., Zakrzewski, V. G.,
376 Voth, G. A., Salvador, P., Dannenberg, J. J., Dapprich, S., Daniels, A. D., Farkas, O., Foresman, J. B., Ortiz, J. V., Cioslowski,
377 J., and Fox, D. J.: *Gaussian 09*, Gaussian Inc., 2009.

378 Ge, X., Wexler, A. S., and Clegg, S. L.: Atmospheric amines – Part I. A review, *Atmos. Environ.*, 45, 524-546,
379 <https://doi.org/10.1016/j.atmosenv.2010.10.012>, 2011.

380 Gentner, D. R., Ormeño, E., Fares, S., Ford, T. B., Weber, R., Park, J. H., Brioude, J., Angevine, W. M., Karlik, J. F., and
381 Goldstein, A. H.: Emissions of terpenoids, benzenoids, and other biogenic gas-phase organic compounds from agricultural
382 crops and their potential implications for air quality, *Atmos. Chem. Phys.*, 14, 5393-5413, [https://doi.org/10.5194/acp-14-](https://doi.org/10.5194/acp-14-5393-2014)
383 5393-2014, 2014.

384 Glowacki, D. R., Liang, C.-H., Morley, C., Pilling, M. J., and Robertson, S. H.: MESMER: An Open-Source Master Equation
385 Solver for Multi-Energy Well Reactions, *J. Phys. Chem. A*, 116, 9545-9560, <https://doi.org/10.1021/jp3051033>, 2012.

386 Guo, X., Ma, F., Liu, C., Niu, J., He, N., Chen, J., and Xie, H. B.: Atmospheric oxidation mechanism and kinetics of isoprene
387 initiated by chlorine radicals: A computational study, *Sci. Total Environ.*, 712, 136330,
388 <https://doi.org/10.1016/j.scitotenv.2019.136330>, 2020.

389 Holbrook, K. A., Pilling, M. J., Robertson, S. H., and Robinson, P. J.: *Unimolecular Reactions*, 2nd ed, Wiley: New York, 1996.

390 Jahn, L. G., Wang, D. S., Dhulipala, S. V., Ruiz, L. H. et al. Gas-phase chlorine radical oxidation of alkanes: Effects of
391 structural branching, NO_x, and relative humidity observed during environmental chamber experiments, *The Journal of Physical*
392 *Chemistry A*, 125(33): 7303-7317, <https://doi.org/10.1021/acs.jpca.1c03516>, 2021.

393 Ji, Y., Wang, H., Gao, Y., Li, G., and An, T. C.: A theoretical model on the formation mechanism and kinetics of highly toxic
394 air pollutants from halogenated formaldehydes reacted with halogen atoms, *Atmos. Chem. Phys.*, 13, 11277-11286,
395 <https://doi.org/10.5194/acp-13-11277-2013>, 2013.

396 Ji, Y., Zheng, J., Qin, D., Li, Y., Gao, Y., Yao, M., Chen, X., Li, G., An, T., and Zhang, R.: OH-Initiated Oxidation of
397 Acetylacetone: Implications for Ozone and Secondary Organic Aerosol Formation, *Environ. Sci. Technol.*, 52, 11169-11177,
398 [10.1021/acs.est.8b03972](https://doi.org/10.1021/acs.est.8b03972), 2018.

399 Ji, Y., Zhao, J., Terazono, H., Misawa, K., Levitt, N. P., Li, Y., Lin, Y., Peng, J., Wang, Y., Duan, L., Pan, B., Zhang, F., Feng,
400 X., An, T., Marrero-Ortiz, W., Secrest, J., Zhang, A. L., Shibuya, K., Molina, M. J., and Zhang, R.: Reassessing the atmospheric
401 oxidation mechanism of toluene, *Proc. Natl. Acad. Sci. U.S.A.*, 114, 8169, [10.1073/pnas.1705463114](https://doi.org/10.1073/pnas.1705463114), 2017.

402 Karl, T., Striednig, M., Graus, M., Hammerle, A., and Wohlfahrt, G.: Urban flux measurements reveal a large pool of
403 oxygenated volatile organic compound emissions, *Proc. Natl. Acad. Sci. U.S.A.*, 115, 1186,
404 <https://doi.org/10.1073/pnas.1714715115>, 2018.

405 Khare, P. and Gentner, D. R.: Considering the future of anthropogenic gas-phase organic compound emissions and the
406 increasing influence of non-combustion sources on urban air quality, *Atmos. Chem. Phys.*, 18, 5391-5413,
407 <https://doi.org/10.5194/acp-18-5391-2018>, 2018.

408 Laskin, A., Smith, J. S., and Laskin, J.: Molecular Characterization of Nitrogen-Containing Organic Compounds in Biomass
409 Burning Aerosols Using High-Resolution Mass Spectrometry, *Environ. Sci. Technol.*, 43, 3764-3771,
410 <https://doi.org/10.1021/es803456n>, 2009.

411 Le Breton, M., Hallquist, Å. M., Pathak, R. K., Simpson, D., Wang, Y., Johansson, J., Zheng, J., Yang, Y., Shang, D., Wang,
412 H., Liu, Q., Chan, C., Wang, T., Bannan, T. J., Priestley, M., Percival, C. J., Shallcross, D. E., Lu, K., Guo, S., Hu, M., and
413 Hallquist, M.: Chlorine oxidation of VOCs at a semi-rural site in Beijing: significant chlorine liberation from ClNO₂ and
414 subsequent gas- and particle-phase Cl-VOC production, *Atmos. Chem. Phys.*, 18, 13013-13030, [https://doi.org/10.5194/acp-](https://doi.org/10.5194/acp-18-13013-2018)
415 [18-13013-2018](https://doi.org/10.5194/acp-18-13013-2018), 2018.

416 Hofzumahaus, A., Rohrer, F., Lu, K., Bohn, B., Brauers, T., Chang, C.-C., Fuchs, H., Holland, F., Kita, K., Kondo, Y., Li, X.,
417 Lou, S., Shao, M., Zeng, L., Wahner, A., and Zhang, Y.: Amplified Trace Gas Removal in the Troposphere, *Science*, 324,
418 1702-1704, <https://doi.org/10.1126/science.1164566>, 2009.

419 Lewis Alastair, C.: The changing face of urban air pollution, *Science*, 359, 744-745, <https://doi.org/10.1126/science.aar4925>,
420 2018.

421 Li, J., Zhang, N., Wang, P., Choi, M., Ying, Q., Guo, S., Lu, K., Qiu, X., Wang, S., Hu, M., Zhang, Y., and Hu, J.: Impacts of
422 chlorine chemistry and anthropogenic emissions on secondary pollutants in the Yangtze river delta region, *Environ. Pollut.*,
423 287, 117624, <https://doi.org/10.1016/j.envpol.2021.117624>, 2021.

424 Li, K., Li, J., Tong, S., Wang, W., Huang, R. J., and Ge, M.: Characteristics of wintertime VOCs in suburban and urban Beijing:
425 concentrations, emission ratios, and festival effects, *Atmos. Chem. Phys.*, 19, 8021-8036, [https://doi.org/10.5194/acp-19-8021-](https://doi.org/10.5194/acp-19-8021-2019)
426 [2019](https://doi.org/10.5194/acp-19-8021-2019), 2019.

427 Lin, Y., Ji, Y., Li, Y., Secrest, J., Xu, W., Xu, F., Wang, Y., An, T., and Zhang, R.: Interaction between succinic acid and
428 sulfuric acid-base clusters, *Atmos. Chem. Phys.*, 19, 8003-8019, <https://doi.org/10.5194/acp-19-8003-2019>, 2019.

429 Ma, F.F., Xie, H.-B., Li, M., Wang, S., Zhang, R., and Chen, J.: Autoxidation mechanism for atmospheric oxidation of tertiary
430 amines: Implications for secondary organic aerosol formation, *Chemosphere*, 273, 129207,
431 <https://doi.org/10.1016/j.chemosphere.2020.129207>, 2021a.

432 Ma, F.F., Xie, H. B., Elm, J., Shen, J., Chen, J., and Vehkamäki, H.: Piperazine Enhancing Sulfuric Acid-Based New Particle
433 Formation: Implications for the Atmospheric Fate of Piperazine, *Environ. Sci. Technol.*, 53, 8785-8795,
434 <https://doi.org/10.1021/acs.est.9b02117>, 2019.

435 Ma, F.F., Guo, X. R., Xia, D. M., Xie, H. B., Wang, Y., Elm, J., Chen, J., and Niu, J.: Atmospheric Chemistry of Allylic
436 Radicals from Isoprene: A Successive Cyclization-Driven Autoxidation Mechanism, *Environ. Sci. Technol.*, 55, 4399-4409,
437 <https://doi.org/10.1021/acs.est.0c07925>, 2021b.

438 Ma, F.F., Ding, Z. Z., Elm, J., Xie, H. B., Yu, Q., Liu, C., Li, C., Fu, Z., Zhang, L., and Chen, J.: Atmospheric Oxidation of
439 Piperazine Initiated by $\cdot\text{Cl}$: Unexpected High Nitrosamine Yield, *Environ. Sci. Technol.*, 52, 9801-9809,
440 <https://doi.org/10.1021/acs.est.8b02510>, 2018a.

441 Ma, F.F., Xie, H. B., and Chen, J.: Benchmarking of DFT functionals for the kinetics and mechanisms of atmospheric addition
442 reactions of OH radicals with phenyl and substituted phenyl-based organic pollutants, *Int. J. Quantum Chem.*, 118, e25533,
443 <https://doi.org/10.1002/qua.25533>, 2018b.

444 Ma, Q., Meng, N., Li, Y., and Wang, J.: Occurrence, impacts, and microbial transformation of 3-methylindole (skatole): A
445 critical review, *J. Hazard. Mater.*, 416, 126181, <https://doi.org/10.1016/j.jhazmat.2021.126181>, 2021b.

446 MacLeod, M., Scheringer, M., Podey, H., Jones, K. C., and Hungerbühler, K.: The Origin and Significance of Short-Term
447 Variability of Semivolatile Contaminants in Air, *Environ. Sci. Technol.*, 41, 3249-3253, <https://doi.org/10.1021/es062135w>,
448 2007.

449 McKee, M. L., Nicolaides, A., and Radom, L.: A Theoretical Study of Chlorine Atom and Methyl Radical Addition to Nitrogen
450 Bases: Why Do Cl Atoms Form Two-Center-Three-Electron Bonds Whereas CH_3 Radicals Form Two-Center-Two-Electron
451 Bonds, *J. Am. Chem. Soc.*, 118, 10571-10576, <https://doi.org/10.1021/ja9613973>, 1996.

452 Misztal, P. K., Hewitt, C. N., Wildt, J., Blande, J. D., Eller, A. S. D., Fares, S., Gentner, D. R., Gilman, J. B., Graus, M.,
453 Greenberg, J., Guenther, A. B., Hansel, A., Harley, P., Huang, M., Jardine, K., Karl, T., Kaser, L., Keutsch, F. N., Kiendler-
454 Scharr, A., Kleist, E., Lerner, B. M., Li, T., Mak, J., Nölscher, A. C., Schnitzhofer, R., Sinha, V., Thornton, B., Warneke, C.,
455 Wegener, F., Werner, C., Williams, J., Worton, D. R., Yassaa, N., and Goldstein, A. H.: Atmospheric benzenoid emissions
456 from plants rival those from fossil fuels, *Sci. Rep.*, 5, 12064, <https://doi.org/10.1038/srep12064>, 2015.

457 Montgomery, J. A., Frisch, M. J., Ochterski, J. W., and Petersson, G. A.: A complete basis set model chemistry. VI. Use of
458 density functional geometries and frequencies, *J. Chem. Phys.*, 110, 2822-2827, <https://doi.org/10.1063/1.477924>, 1999.

459 Montoya-Aguilera, J., Horne, J. R., Hinks, M. L., Fleming, L. T., Perraud, V., Lin, P., Laskin, A., Laskin, J., Dabdub, D., and
460 Nizkorodov, S. A.: Secondary organic aerosol from atmospheric photooxidation of indole, *Atmos. Chem. Phys.*, 17, 11605-
461 11621, <https://doi.org/10.5194/acp-17-11605-2017>, 2017.

462 Nicovich, J. M., Mazumder, S., Laine, P. L., Wine, P. H., Tang, Y., Bunkan, A. J. C., and Nielsen, C. J.: An experimental and
463 theoretical study of the gas phase kinetics of atomic chlorine reactions with CH_3NH_2 , $(\text{CH}_3)_2\text{NH}$, and $(\text{CH}_3)_3\text{N}$, *Phys. Chem.*
464 *Chem. Phys.*, 17, 911-917, <https://doi.org/10.1039/C4CP03801K>, 2015.

465 Nielsen, C. J., Herrmann, H., and Weller, C.: Atmospheric chemistry and environmental impact of the use of amines in carbon
466 capture and storage (CCS), *Chem. Soc. Rev.*, 41, 6684-6704, <https://doi.org/10.1039/C2CS35059A>, 2012.

467 Onel, L., Dryden, M., Blitz, M. A., and Seakins, P. W.: Atmospheric Oxidation of Piperazine by OH has a Low Potential to
468 Form Carcinogenic Compounds, *Environ. Sci. Technol. Lett.*, 1, 367-371, <https://doi.org/10.1021/ez5002159>, 2014a.

469 Onel, L., Blitz, M., Dryden, M., Thonger, L., and Seakins, P.: Branching Ratios in Reactions of OH Radicals with Methylamine,
470 Dimethylamine, and Ethylamine, *Environ. Sci. Technol.*, 48, 9935-9942, <https://doi.org/10.1021/es502398r>, 2014b.

471 Praske, E., Otkjær, R. V., Crounse, J. D., Hethcox, J. C., Stoltz, B. M., Kjaergaard, H. G., and Wennberg, P. O.: Atmospheric
472 autoxidation is increasingly important in urban and suburban North America, *Proc. Natl. Acad. Sci. U.S.A.*, 115, 64,
473 <https://doi.org/110.1073/pnas.1715540115>, 2018.

474 Reed, A. E., Weinstock, R. B., and Weinhold, F.: Natural population analysis, *J. Chem. Phys.*, 83, 735-746,
475 <https://doi.org/10.1063/1.449486>, 1985.

476 Ren, Z. and da Silva, G.: Atmospheric Oxidation of Piperazine Initiated by OH: A Theoretical Kinetics Investigation, *ACS*
477 *Earth Space Chem.*, 3, 2510-2516, <https://doi.org/10.1021/acsearthspacechem.9b00227>, 2019.

478 Riedel, T. P., Bertram, T. H., Crisp, T. A., Williams, E. J., Lerner, B. M., Vlasenko, A., Li, S.-M., Gilman, J., de Gouw, J.,
479 Bon, D. M., Wagner, N. L., Brown, S. S., and Thornton, J. A.: Nitryl Chloride and Molecular Chlorine in the Coastal Marine
480 Boundary Layer, *Environ. Sci. Technol.*, 46, 10463-10470, <https://doi.org/10.1021/es204632r>, 2012.

481 Rienstra-Kiracofe, J. C., Allen, W. D., and Schaefer, H. F.: The $C_2H_5 + O_2$ Reaction Mechanism: High-Level ab Initio
482 Characterizations, *J. Phys. Chem. A*, 104, 9823-9840, <https://doi.org/10.1021/jp001041k>, 2000.

483 Robinson, P. J., and Holbrook, K. A.: *Unimolecular Reactions*, John Wiley & Sons: New York, 1972.

484 SenGupta, S., Indulkar, Y., Kumar, A., Dhanya, S., Naik, P. D., and Bajaj, P. N.: Kinetics of Gas-Phase Reaction of OH with
485 Morpholine: An Experimental and Theoretical Study, *J. Phys. Chem. A*, 114, 7709-7715, <https://doi.org/10.1021/jp101464x>,
486 2010.

487 Schade, G. W. and Crutzen, P. J.: Emission of aliphatic amines from animal husbandry and their reactions: Potential source of
488 N_2O and HCN, *J. Atmos. Chem.*, 22, 319-346, <https://doi.org/10.1007/BF00696641>, 1995.

489 Shiels, O. J., Kelly, P. D., Bright, C. C., Poad, B. L. J., Blanksby, S. J., da Silva, G., and Trevitt, A. J.: Reactivity Trends in the
490 Gas-Phase Addition of Acetylene to the N-Protonated Aryl Radical Cations of Pyridine, Aniline, and Benzonitrile, *J. Am. Soc.*
491 *Mass. Spectrom.*, 32, 537-547, <https://doi.org/10.1021/jasms.0c00386>, 2021.

492 Shen, J., Elm, J., Xie, H.-B., Chen, J., Niu, J., and Vehkamäki, H.: Structural Effects of Amines in Enhancing Methanesulfonic
493 Acid-Driven New Particle Formation, *Environ. Sci. Technol.*, 54, 13498-13508, <https://doi.org/10.1021/acs.est.0c05358>, 2020.

494 Shen, J., Xie, H.-B., Elm, J., Ma, F., Chen, J., and Vehkamäki, H.: Methanesulfonic Acid-driven New Particle Formation
495 Enhanced by Monoethanolamine: A Computational Study, *Environ. Sci. Technol.*, 53, 14387-14397,
496 <https://doi.org/10.1021/acs.est.9b05306>, 2019.

497 Silva, P. J., Erupe, M. E., Price, D., Elias, J., G. J. Malloy, Q., Li, Q., Warren, B., and Cocker, D. R.: Trimethylamine as
498 Precursor to Secondary Organic Aerosol Formation via Nitrate Radical Reaction in the Atmosphere, *Environ. Sci. Technol.*,
499 42, 4689-4696, <https://doi.org/10.1021/es703016v>, 2008.

500 Tan, W., Zhu, L., Mikoviny, T., Nielsen, C. J., Wisthaler, A., D'Anna, B., Antonsen, S., Stenstrøm, Y., Farren, N. J., Hamilton,
501 J. F., Boustead, G. A., Brennan, A. D., Ingham, T., and Heard, D. E.: Experimental and Theoretical Study of the OH-Initiated
502 Degradation of Piperazine under Simulated Atmospheric Conditions, *J. Phys. Chem. A*, 125, 411-422,
503 <https://doi.org/10.1021/acs.jpca.0c10223>, 2021.

504 Thornton, J. A., Kercher, J. P., Riedel, T. P., Wagner, N. L., Cozic, J., Holloway, J. S., Dubé, W. P., Wolfe, G. M., Quinn, P.
505 K., Middlebrook, A. M., Alexander, B., and Brown, S. S.: A large atomic chlorine source inferred from mid-continental
506 reactive nitrogen chemistry, *Nature*, 464, 271-274, <https://doi.org/10.1038/nature08905>, 2010.

507 Veres, P. R., Neuman, J. A., Bertram, T. H., Assaf, E., Wolfe, G. M., Williamson, C. J., Weinzierl, B., Tilmes, S., Thompson,
508 C. R., Thames, A. B., Schroder, J. C., Saiz-Lopez, A., Rollins, A. W., Roberts, J. M., Price, D., Peischl, J., Nault, B. A., Møller,
509 K. H., Miller, D. O., Meinardi, S., Li, Q., Lamarque, J.-F., Kupc, A., Kjaergaard, H. G., Kinnison, D., Jimenez, J. L., Jernigan,
510 C. M., Hornbrook, R. S., Hills, A., Dollner, M., Day, D. A., Cuevas, C. A., Campuzano-Jost, P., Burkholder, J., Bui, T. P.,
511 Brune, W. H., Brown, S. S., Brock, C. A., Bourgeois, I., Blake, D. R., Apel, E. C., and Ryerson, T. B.: Global airborne sampling
512 reveals a previously unobserved dimethyl sulfide oxidation mechanism in the marine atmosphere, *Proc. Natl. Acad. Sci. U.S.A.*,
513 117, 4505, <https://doi.org/10.1073/pnas.1919344117>, 2020.

514 Wang, S. and Wang, L.: The atmospheric oxidation of dimethyl, diethyl, and diisopropyl ethers. The role of the intramolecular
515 hydrogen shift in peroxy radicals, *Phys. Chem. Chem. Phys.*, 18, 7707-7714, <https://doi.org/10.1039/C5CP07199B>, 2016.

516 Wang, S., Riva, M., Yan, C., Ehn, M., and Wang, L.: Primary Formation of Highly Oxidized Multifunctional Products in the
517 OH-Initiated Oxidation of Isoprene: A Combined Theoretical and Experimental Study, *Environ. Sci. Technol.*, 52, 12255-
518 12264, <https://doi.org/10.1021/acs.est.8b02783>, 2018.

519 Wang, S., Wu, R., Berndt, T., Ehn, M., and Wang, L.: Formation of Highly Oxidized Radicals and Multifunctional Products
520 from the Atmospheric Oxidation of Alkylbenzenes, *Environ. Sci. Technol.*, 51, 8442-8449,
521 <https://doi.org/10.1021/acs.est.7b02374>, 2017.

522 Wang, K., Wang, W. G., Fan, C. C.: Reactions of C₁₂-C₁₄ N-Alkylcyclohexanes with Cl Atoms: Kinetics and Secondary
523 Organic Aerosol Formation, *Environ. Sci. Technol.*, 56(8): 4859-4870, <https://doi.org/10.1021/acs.est.1c08958>, 2022.

524 Wu, R., Wang, S., and Wang, L.: New Mechanism for the Atmospheric Oxidation of Dimethyl Sulfide. The Importance of
525 Intramolecular Hydrogen Shift in a CH₃SCH₂OO Radical, *J. Phys. Chem. A*, 119, 112-117, <https://doi.org/10.1021/jp511616j>,
526 2015.

527 Xia, M., Peng, X., Wang, W.: Significant Production of ClNO₂ and Possible Source of Cl₂ from N₂O₅ Uptake at a Suburban
528 Site in Eastern China, *Atmos. Chem. Phys.*, 20(10): 6147-6158, <https://doi.org/10.1021/10.5194/acp-20-6147-2020>, 2020.

529 Xie, H. B., Ma, F.F., Yu, Q., He, N., and Chen, J. W.: Computational Study of the Reactions of Chlorine Radicals with
530 Atmospheric Organic Compounds Featuring NH_x - π -Bond ($x = 1, 2$) Structures, *J. Phys. Chem. A*, 121, 1657-1665,
531 <https://doi.org/10.1021/acs.jpca.6b11418>, 2017.

532 Xie, H. B., Li, C., He, N., Wang, C., Zhang, S., and Chen, J. W.: Atmospheric Chemical Reactions of Monoethanolamine
533 Initiated by OH Radical: Mechanistic and Kinetic Study, *Environ. Sci. Technol.*, 48, 1700-1706,
534 <https://doi.org/10.1021/es405110t>, 2014.

535 Xie, H. B., Ma, F.F., Wang, Y., He, N., Yu, Q., and Chen, J. W.: Quantum Chemical Study on $\cdot\text{Cl}$ -Initiated Atmospheric
536 Degradation of Monoethanolamine, *Environ. Sci. Technol.*, 49, 13246-13255, <https://doi.org/10.1021/acs.est.5b03324>, 2015.

537 Young, C. J., Washenfelder, R. A., Edwards, P. M., Parrish, D. D., Gilman, J. B., Kuster, W. C., Mielke, L. H., Osthoff, H. D.,
538 Tsai, C., Pikelnaya, O., Stutz, J., Veres, P. R., Roberts, J. M., Griffith, S., Dusanter, S., Stevens, P. S., Flynn, J., Grossberg,
539 N., Lefer, B., Holloway, J. S., Peischl, J., Ryerson, T. B., Atlas, E. L., Blake, D. R., and Brown, S. S.: Chlorine as a primary
540 radical: evaluation of methods to understand its role in initiation of oxidative cycles, *Atmos. Chem. Phys.*, 14, 3427-3440,
541 <https://doi.org/10.5194/acp-14-3427-2014>, 2014.

542 Yu, D., Tan, Z., Lu, K., Ma, X., Li, X., Chen, S., Zhu, B., Lin, L., Li, Y., Qiu, P., Yang, X., Liu, Y., Wang, H., He, L., Huang,
543 X., and Zhang, Y.: An explicit study of local ozone budget and NO_x -VOCs sensitivity in Shenzhen China, *Atmos. Environ.*,
544 224, 117304, <https://doi.org/10.1016/j.atmosenv.2020.117304>, 2020.

545 Yu, F. and Luo, G.: Modeling of gaseous methylamines in the global atmosphere: impacts of oxidation and aerosol uptake,
546 *Atmos. Chem. Phys.*, 14, 12455-12464, <https://doi.org/10.5194/acp-14-12455-2014>, 2014.

547 Yu, Q., Xie, H. B., and Chen, J. W.: Atmospheric chemical reactions of alternatives of polybrominated diphenyl ethers initiated
548 by OH: A case study on triphenyl phosphate, *Sci. Total Environ.*, 571, 1105-1114,
549 <https://doi.org/10.1016/j.scitotenv.2016.07.105>, 2016.

550 Yu, Q., Xie, H. B., Li, T., Ma, F., Fu, Z., Wang, Z., Li, C., Fu, Z., Xia, D., and Chen, J. W.: Atmospheric chemical reaction
551 mechanism and kinetics of 1,2-bis(2,4,6-tribromophenoxy)ethane initiated by OH radical: a computational study, *RSC Adv.*,
552 7, 9484-9494, <https://doi.org/10.1039/C6RA26700A>, 2017.

553 Yuan, B., Coggon, M. M., Koss, A. R., Warneke, C., Eilerman, S., Peischl, J., Aikin, K. C., Ryerson, T. B., and de Gouw, J.
554 A.: Emissions of volatile organic compounds (VOCs) from concentrated animal feeding operations (CAFOs): chemical
555 compositions and separation of sources, *Atmos. Chem. Phys.*, 17, 4945-4956, <https://doi.org/10.5194/acp-17-4945-2017>, 2017.

556 Zhang, R., Wang, G., Guo, S., Zamora, M. L., Ying, Q., Lin, Y., Wang, W., Hu, M., and Wang, Y.: Formation of Urban Fine
557 Particulate Matter, *Chem. Rev.*, 115, 3803-3855, <https://doi.org/10.1021/acs.chemrev.5b00067>, 2015.

558 Zhang, Z., Lin, L., and Wang, L.: Atmospheric oxidation mechanism of naphthalene initiated by OH radical. A theoretical
559 study, *Phys. Chem. Chem. Phys.*, 14, 2645-2650, <https://doi.org/10.1039/C2CP23271E>, 2012.

560 Zhao, Y. and Truhlar, D. G.: The M06 suite of density functionals for main group thermochemistry, thermochemical kinetics,
561 noncovalent interactions, excited states, and transition elements: two new functionals and systematic testing of four M06-class
562 functionals and 12 other functionals, *Theor. Chem. Acc.*, 120, 215-241, <https://doi.org/10.1007/s00214-007-0310-x>, 2008.

- 563 Zito, P., Dötterl, S., and Sajeва, M.: Floral Volatiles in a Sapromyiophilous Plant and Their Importance in Attracting House
564 Fly Pollinators, *J. Chem. Ecol.*, 41, 340-349, <https://doi.org/10.1007/s10886-015-0568-8>, 2015.